Supporting information:

Photolytic studies of Norbornadiene Derivatives Under High-intensity Light Conditions

Alexander Kjaersgaard,[†] Helen Hölzel,[‡] Kasper Moth-Poulsen,[‡] and Mogens Brøndsted Nielsen[*,†]

[†]*Department of Chemistry, University of Copenhagen, Universitetsparken 5, DK-2100 Copenhagen, Denmark*

[‡]*Department of Chemistry and Chemical Engineering, Chalmers University of Technology, Kemigården, Gothenburg 41296, Sweden*

E-mail: mbn@chem.ku.dk

Contents

S1 FTIR spectra

FTIR spectra were recorded in the 2000-2400 cm^{-1} range to observe the fundamental nitrile stretching band of the NBD and QC derivative used here. Spectra were recorded of a 0.100 M solution in a 0.025 mm cell with NaCl windows on a VERTEX 80 spectrometer (Bruker) equipped with a MIR light source, a liquid nitrogen cooled MCT detector and a CaF_2 beamsplitter. The spectra were averaged over 1000 scans with a 1 cm^{-1} resolution, a Blackman-Harris 3 term apodization, a Mertz phase correction and an 80 kHz scanner velocity. The spectra were recorded with a short path length to minimize the influence of the toluene solvent. While only relatively weak combination and hot-bands of toulene exist in the 2000 - 2400 cm^{-1} region, these bands still saturate the spectrum if recorded with a 1-cm cuvette, due to its high neat concentration. However, due to the short optical path length, a suitably high concentration of NBD/QC must be used to observe their nitrile stretching bands.

In Figure S1, we show the recorded FTIR spectra of the fundamental nitrile stretching bands of NBD (blue) and QC (red). The spectrum of NBD was recorded after the sample had cooled down from two hours of heating at 343 K, and the spectrum of QC was recorded after being irradiated at 340 nm for four hours with the OPO-laser. The nitrile stretch of NBD (2196 cm^{-1}) is observed in the blue trace, while that of QC (2222 cm^{-1}) is not, showing that all of the MOST fluid is in the NBD form after being heated. After four hours of irradiation at 340 nm ($\sim$ 22 mW), the absorbance of the nitrile band of QC is seen to increase, while that of NBD decreases.

The ratio of the absorbance at 2196 cm^{-1} before (0.806) and after (0.00157) irradiation is 1.9%, which means that at most, under 2% NBD is present at equilibrium. However, due to the overlap with the nitrile band of QC, this is likely less.

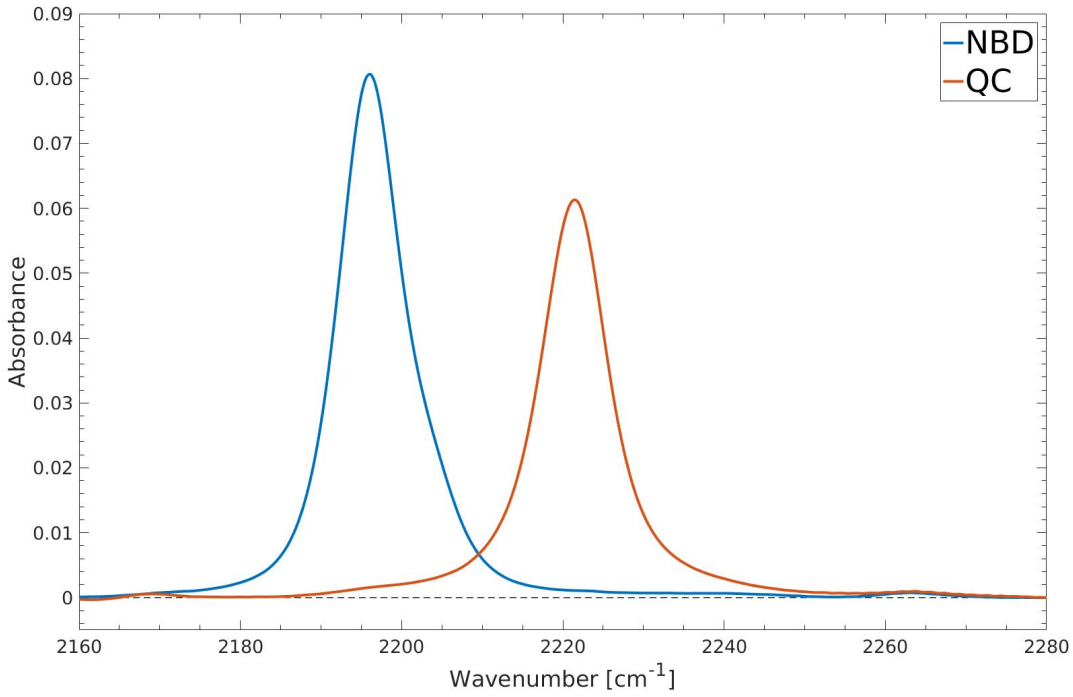

Figure S1: FTIR spectrum of the fundamental nitrile stretch of NBD (blue) and QC (red). Initial concentration of 1.00×10^{-1} M and recorded with 0.025 mm optical path length. Peak maximum of the nitrile stretch of NBD at 2196 cm^{-1} with absorbance of 0.08067 and 0.00157, before and after irradiation, respectively. Peak maximum of the nitrile stretch of QC at 2222 cm^{-1} with absorbance of 0.00109 and 0.0613, before and after irradiation, respectively.

S2 Correction for reflected light

When measuring the laser power, part of the light was observed to be reflected off of the pyroelectric sensor. Due to this, the sensor likely underestimates the true laser power, which in turn overestimates $\phi_{NBD \rightarrow QC}$. To a good approximation, the total laser power is the sum of the absorbed and reflected light from the sensor. To measure the amount of light reflected off of the pyroelectric sensor, we placed the probe of the SolarRad close to the pyroelectric sensor (3.0 cm) and slightly off-set from the laser beam, which was set to 340 nm. The measurement was performed in darkness. In Figure S2, the spectrum measured on the SolarRad is shown. A clear peak at 340 nm is seen (FWHM at 3.4 nm), as well as a small laser impurity at 679 nm.

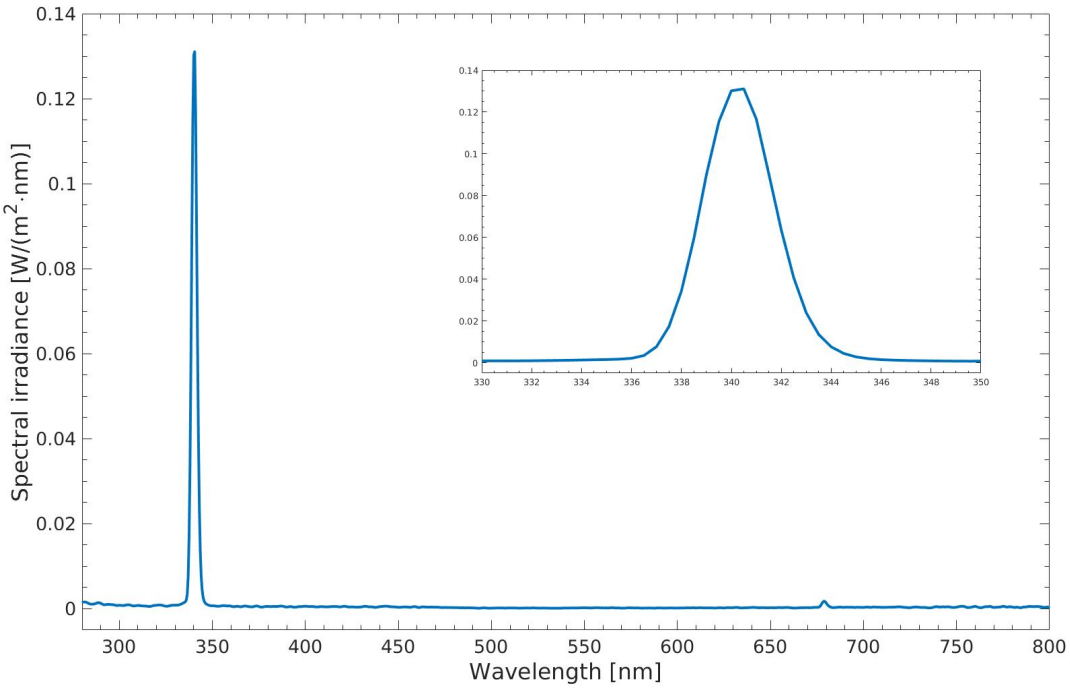

Figure S2: Spectrum of the OPO-laser at 340 nm reflected off of the pyroelectric sensor.

The irradiance of the peak at 340 nm is 0.49 W/m^2. If the reflection occurs equally in all directions, the total reflected laser power can be calculated by multiplying the irradiance with the surface area of a hemisphere with a radius of 3 cm. This gives a total reflected power of 0.00276 W. The measured power on the pyroelectric sensor was 0.0252 W, giving a reflectivity of $\sim 11\%$.

S3 Ferrioxalate actinometry

The calibration of the pyroelectric sensor was checked by comparing photon fluxes of the sensor to that determined using ferrioxalate actinometry.[1,2] We follow the method described by Stranius and Börjesson.[3] In short, a solution of ferrioxalate (3.06×10^{-2} M in 0.2 N H_2SO_4) was prepared. An aliquot of 3.0 mL (V_1) was transferred to a 1-cm quartz cuvette, which was irradiated at 340 nm under stirring (900 RPM). After irradiation, 0.6 mL (V_2) of the solution in the cuvette was transferred to a 50 mL (V_3) volumetric flask, and 1.0 mL

buffer (1.18 M Na + 0.72 N H_2SO_4) and 2.0 mL phenanthanroline (5.90 mM) were added, and the solution was diluted with milliQ water to the 50 mL mark. This was repeated five times, with irradiation times between 0 and 120 seconds in steps of 30 seconds. The cuvette was rinsed with milliQ water and dried between each measurement. Measurements were performed in total darkness with a red LED headlight, as red light does not decompose ferrioxalate.[1,2] The diluted 50 mL solutions were left to react in darkness for one hour, after which absorption spectra of the tris-phenanthroline-iron(II) complex could be observed at 510 nm ($\epsilon_{510nm} = 11000$ $M^{-1}cm^{-1}$).[3] The photon flux (I), in s^{-1}, was then determined by eq. (S1).

$$I = \frac{dAbs}{dt_{irr}} \times \frac{V_1 \times V_3}{V_2 \times \epsilon_{510nm} \times l \times \phi}. \tag{S1}$$

Here, $\frac{dAbs}{dt_{irr}}$ is the slope of a linear fit of the absorbance at 510 nm against the irradiation time, l is the cuvette path length of 1 cm, and ϕ is the quantum yield of ferrioxalate decomposition,[3] which at 340 nm is 1.23. In the left panel of Figure S3, we show the absorption spectra of tris-phenanthroline-iron(II) at different irradiation times. A higher absorbance is observed in the spectra with longer irradiation time. In the right panel, we show the linear correlation between the absorbance and irradiation time. These data are also given in Table S1. From eq. (S1) a photon flux of 3.94×10^{16} s^{-1} was determined. After the ferrioxalate measurements, a photon flux of 4.07×10^{16} s^{-1} was measured with the pyroelectric sensor. The two approaches are in good agreement, deviating less than 4%.

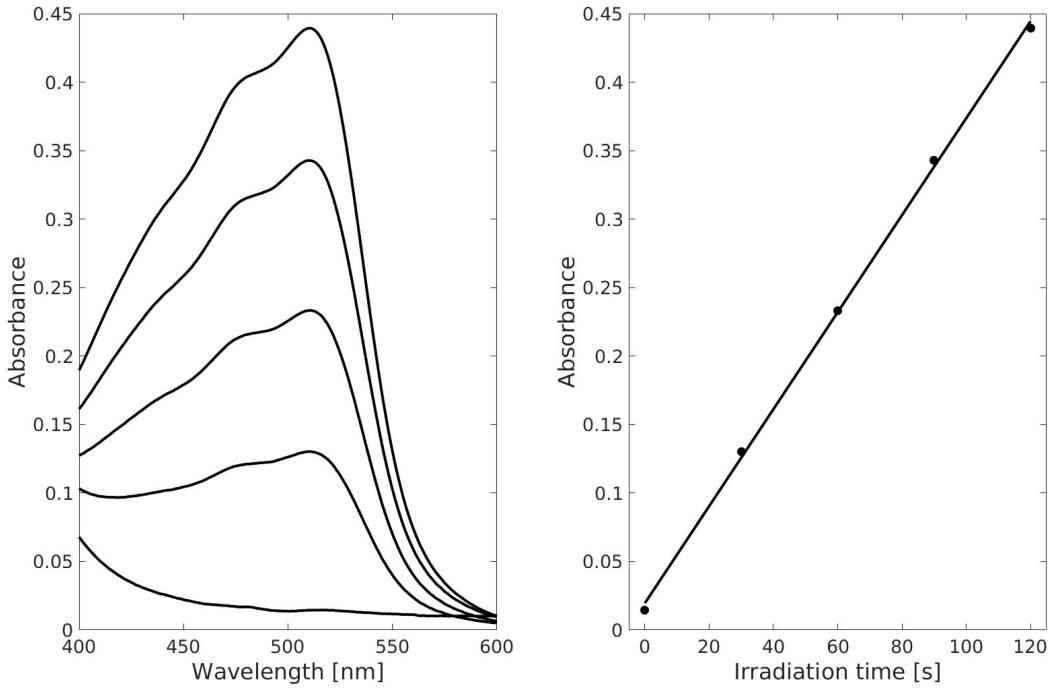

Figure S3: **Left**: Absorption spectra of tris-phenanthroline-iron(II) at different irradiation times. **Right**: Irradiation times against the absorbance at 510 nm.

Table S1: Irradition time (t_{irr}) in seconds and absorbance at 510 nm (Abs) of a ferrioxalate solution irradiation at 340 nm.

t_{irr}	Abs
0	0.0145
30	0.130
60	0.232
90	0.3427
120	0.440

S4 Photoisomerization quantum yield

S4.1 Uncertainty propagation

Using standard error propagation, the relative uncertainty in the concentration (C) can be propagated from the uncertainties in mass (m) and volume (V) as

$$\frac{\sigma_C}{C} = \sqrt{\left(\frac{\sigma_m}{m}\right)^2 + \left(\frac{\sigma_V}{V}\right)^2}, \tag{S2}$$

where σ_C, σ_m and σ_V are the uncertainties of the concentration, mass and volume, respectively. The precision balance had an uncertainty in the mass of $\sigma_m = 0.1$ mg. Volumetric flasks were labeled to within 1% (i.e. $\frac{\sigma_V}{V} = 0.01$). As $\phi_{NBD \rightarrow QC}$ depends proportionally on the concentration, the total uncertainty on ϕ is

$$\phi_{NBD \rightarrow QC} \pm \left(\sigma_{\phi_{fit}} + \sigma_{\phi_{con}}\right). \tag{S3}$$

Here, $\sigma_{\phi_{fit}}$ is the uncertainty obtained in the fitting of the NBD concentration against irradiation time, and $\sigma_{\phi_{con}} = \phi_{NBD \rightarrow QC} \times \frac{\sigma_C}{C}$ is the uncertainty due to concentration.

S4.2 Photoisomerization quantum yield at different stirring rates

Values of $\phi_{NBD \rightarrow QC}$ were determined of a 1.06×10^{-2} M solution with stirring rates of 450, 600, 750 and 900 RPM of the magnetic teflon bar. If the solution is inadequately stirred, the solution will be inhomogeneous. For the NBD/QC derivative used here, the molar absorption coefficients of QC and NBD at 326 nm is 150.3 $M^{-1}cm^{-1}$ and 13200 $M^{-1}cm^{-1}$, respectively. While the absorption of QC is low relative to NBD, a 0.01 M solution of QC in a 1-cm cuvette would give a fairly significant absorbance of 1.5. If the solution is inhomogeneous, pockets of QC will form and block parts of the light, where the irradiation source hits the sample. This increases the time it takes to convert NBD to QC and in turn artificially decreases $\phi_{NBD \rightarrow QC}$. If similar values of $\phi_{NBD \rightarrow QC}$ are determined at different stirring rates, the solution is homogenized and QC blocking part of the light can be accounted for.

Figure S4 shows $\phi_{NBD \rightarrow QC}$ determined at different stirring rates for the 1.06×10^{-2} M solution. Similar value of $\phi_{NBD \rightarrow QC}$ of $\sim$0.8 were observed with different stirring rates. As such, the use of 900 RPM is sufficient to homogenize the solution and avoid inner filter effects.

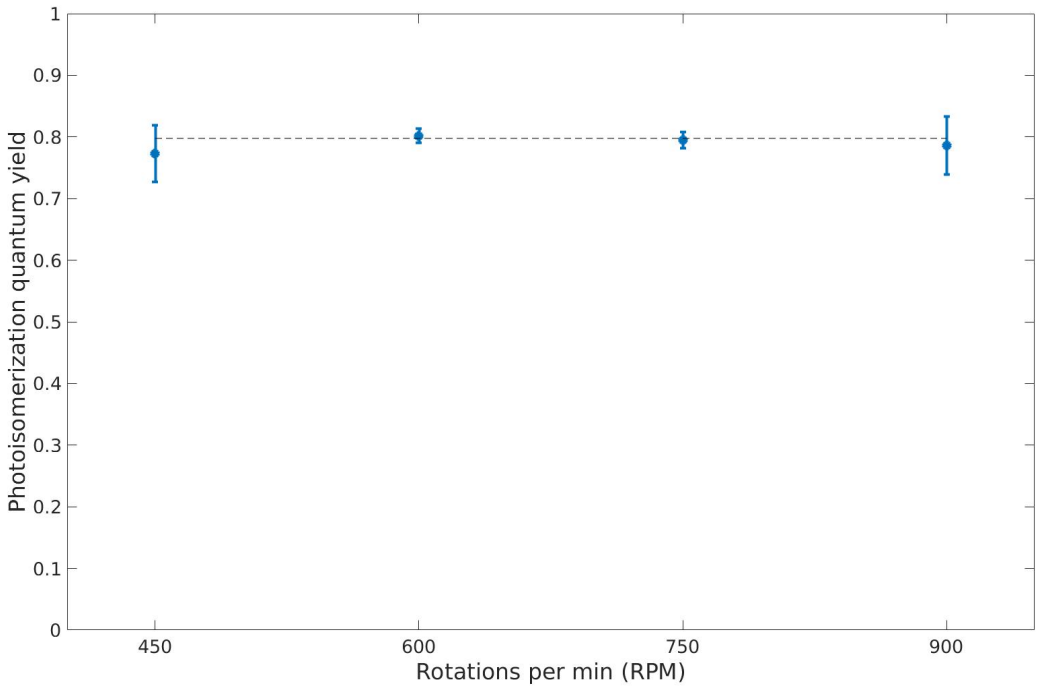

Figure S4: Determined $\phi_{NBD \rightarrow QC}$ values of a 1.06×10^{-2} M solution against stirring rate (using magnetic teflon stirring bar). An average of $\phi_{NBD \rightarrow QC} = 0.80$ is obtained (dashed line).

S4.3 Concentration dependence of the photoisomerization quantum yield

Figure S5 shows the concentration dependence of $\phi_{NBD \rightarrow QC}$ with a linear x-axis. The figure is similar to Figure 3 in the main text where a logarithmic x-axis is used.

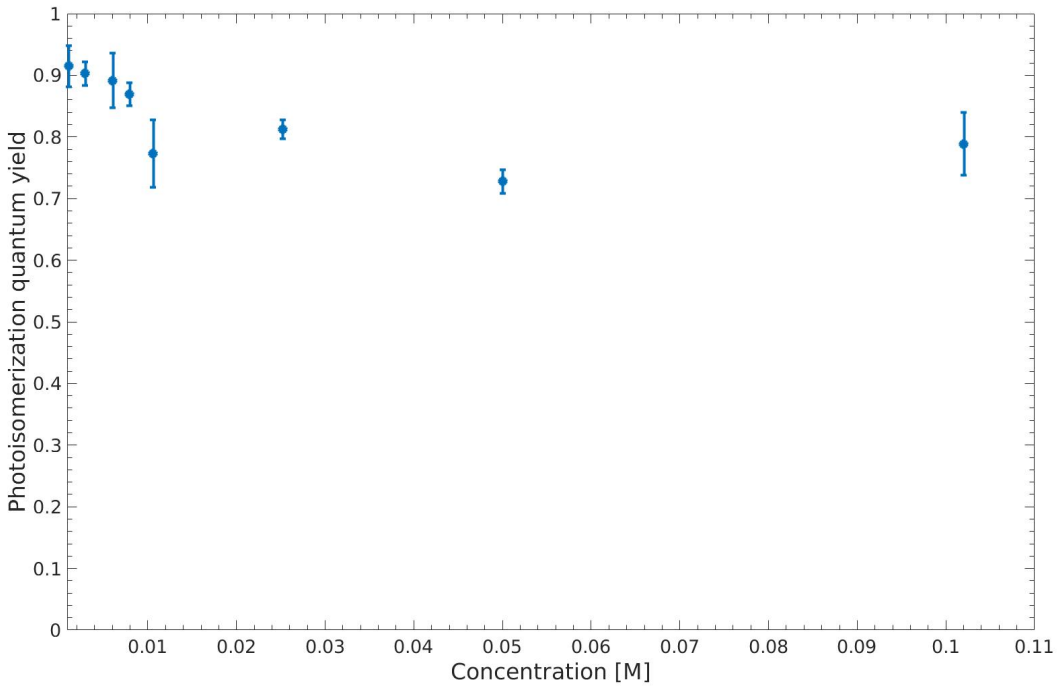

Figure S5: Plot of the photoisomerization quantum yield ($\phi_{NBD \rightarrow QC}$) against initial NBD concentration.

S5 Experimental data using OPO-laser

Table S2: Overview and selected parameters of all experiments using the OPO-laser with experiments labeled A to L. Total concentration (C_{total}, in M), photoisomerization quantum yield ($\phi_{NBD\rightarrow QC}$, unitless), fitting and concentration uncertainties on $\phi_{NBD\rightarrow QC}$ (σ_ϕ, unitless) and irradiation wavelength (λ_{irr}, in nm).

Experiment	C_{total}	$\phi_{NBD\rightarrow QC}$	σ_ϕ[a]	λ_{irr}	Table[b]
A	$(1.08 \pm 0.02) \times 10^{-3}$	0.91 ± 0.03	(0.013)[0.021]	340	S3
B	$(2.93 \pm 0.05) \times 10^{-3}$	0.90 ± 0.02	(0.004)[0.016]	340	S4
C	$(6.05 \pm 0.22) \times 10^{-3}$	0.89 ± 0.04	(0.011)[0.033]	340	S5
D	$(7.95 \pm 0.14) \times 10^{-3}$	0.87 ± 0.02	(0.003)[0.015]	340	S6
E	$(1.06 \pm 0.01) \times 10^{-2}$	0.77 ± 0.05	(0.046)[0.008]	340	S7
F	$(2.52 \pm 0.04) \times 10^{-2}$	0.81 ± 0.02	(0.001)[0.014]	340	S8
G	$(5.00 \pm 0.05) \times 10^{-2}$	0.73 ± 0.02	(0.011)[0.008]	340	S9
H	$(1.02 \pm 0.01) \times 10^{-1}$	0.79 ± 0.05	(0.043)[0.008]	340	S10
I	$(1.08 \pm 0.02) \times 10^{-3}$	0.86 ± 0.02	(0.005)[0.020]	310	S11
J	$(1.08 \pm 0.02) \times 10^{-3}$	0.96 ± 0.03	(0.007)[0.022]	320	S12
K	$(1.08 \pm 0.02) \times 10^{-3}$	0.89 ± 0.02	(0.003)[0.020]	330	S13
L	$(1.08 \pm 0.02) \times 10^{-3}$	0.82 ± 0.03	(0.007)[0.019]	350	S14

a: Values in parentheses and square brackets refer to fitting (at 95% confidence) and concentration uncertainties on $\phi_{NBD\rightarrow QC}$, respectively.
b: Experiment specific information given in respective tables.

Table S3: Data for experiment A. Irradiation time (t_{irr}) in seconds, absorbance at 366 nm (Abs) and molarity of NBD (C_{NBD}). Laser irradiation at 340 nm.

t_{irr}	Abs	C_{NBD}
0	0.982	1.08×10^{-3}
5	0.875	9.60×10^{-4}
10	0.763	8.35×10^{-4}
15	0.655	7.15×10^{-4}
20	0.541	5.88×10^{-4}
25	0.427	4.60×10^{-4}
30	0.309	3.29×10^{-4}
35	0.196	2.03×10^{-4}
40	0.105	1.01×10^{-4}
45	0.049	3.91×10^{-5}
50	0.025	1.23×10^{-5}
55	0.015	1.52×10^{-6}
60	0.014	0

C_{total} = 0.00108 M, $\epsilon_{NBD,366nm}$ = 909.52 $M^{-1}cm^{-1}$, $\epsilon_{QC,366nm}$ = 13.078 $M^{-1}cm^{-1}$, V = 0.00246 L, I = 0.02377 W, l = 1 cm.

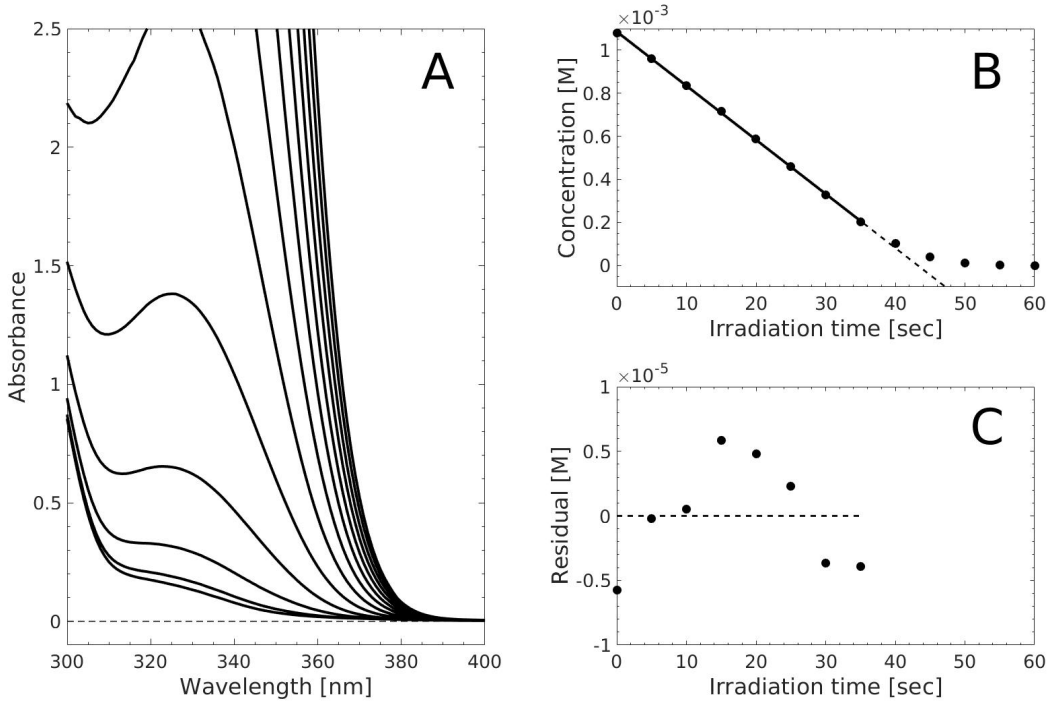

Figure S6: Experimental data plotted for experiment A from Table S3. **A**: Absorption spectra at various irradiation times. **B**: Concentration of NBD against irradiation time. **C**: Residual plot of the linear fit in panel B.

Table S4: Data for experiment B. Irradiation time (t_{irr}) in seconds, absorbance at 373 nm (Abs) and molarity of NBD (C_{NBD}). Laser irradiation at 340 nm.

t_{irr}	Abs	C_{NBD}
0	0.860	2.93×10^{-3}
8	0.807	2.73×10^{-3}
16	0.747	2.51×10^{-3}
24	0.688	2.29×10^{-3}
32	0.630	2.07×10^{-3}
40	0.571	1.85×10^{-3}
48	0.513	1.63×10^{-3}
56	0.455	1.42×10^{-3}
64	0.397	1.20×10^{-3}
72	0.339	9.86×10^{-4}
80	0.280	7.68×10^{-4}
88	0.224	5.60×10^{-4}
96	0.168	3.51×10^{-4}
104	0.118	1.62×10^{-4}
112	0.087	4.89×10^{-5}
120	0.077	1.01×10^{-5}
128	0.074	0
136	0.075	1.56×10^{-6}
144	0.075	4.22×10^{-6}

$C_{total} = 2.93 \times 10^{-3}$ M, $\epsilon_{NBD,373nm} = 293.67$ $M^{-1}cm^{-1}$, $\epsilon_{QC,373nm} = 25.34$ $M^{-1}cm^{-1}$, $V = 0.00244$ L, $I = 0.0258$ W, $l = 1$ cm.

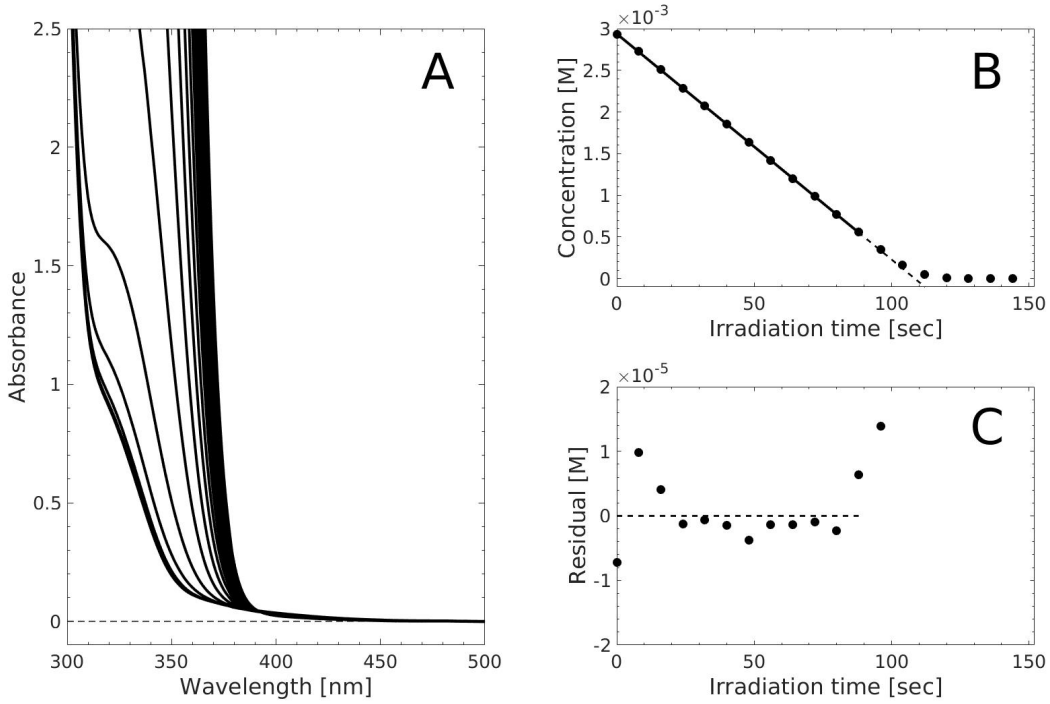

Figure S7: Experimental data plotted for experiment B from Table S4. **A**: Absorption spectra at various irradiation times. **B**: Concentration of NBD against irradiation time. **C**: Residual plot of the linear fit in panel B.

Table S5: Data for experiment C. Irradiation time (t_{irr}) in seconds, absorbance at 376 nm (Abs) and molarity of NBD (C_{NBD}). Laser irradiation at 340 nm.

t_{irr}	Abs	C_{NBD}
0	0.996	6.05×10^{-3}
20	0.890	5.38×10^{-3}
40	0.777	4.66×10^{-3}
60	0.664	3.95×10^{-3}
80	0.548	3.21×10^{-3}
100	0.431	2.48×10^{-3}
120	0.315	1.74×10^{-3}
140	0.199	1.01×10^{-3}
160	0.085	2.89×10^{-4}
180	0.040	5.10×10^{-6}
200	0.039	9.78×10^{-7}
220	0.040	2.52×10^{-6}
240	0.039	0

$C_{total} = 6.05 \times 10^{-3}$ M, $\epsilon_{NBD,376nm} = 164.63$ $M^{-1}cm^{-1}$, $\epsilon_{QC,376nm} = 6.49$ $M^{-1}cm^{-1}$, $V = 0.00185$ L, $I = 0.0264$ W, $l = 1$ cm.

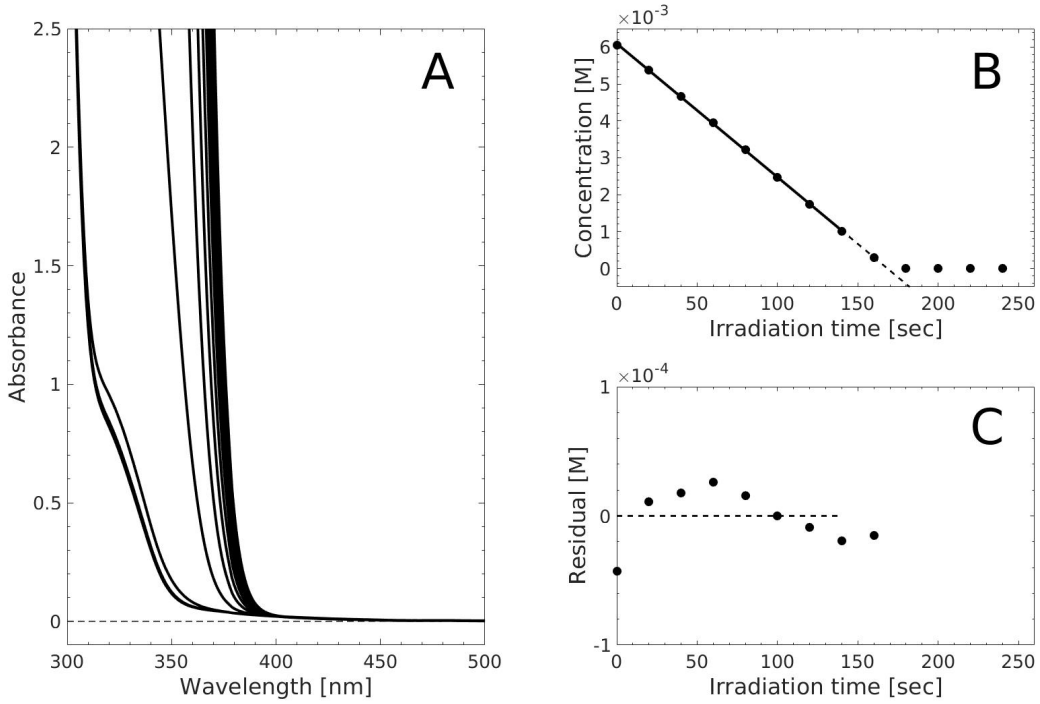

Figure S8: Experimental data plotted for experiment C from Table S5. **A**: Absorption spectra at various irradiation times. **B**: Concentration of NBD against irradiation time. **C**: Residual plot of the linear fit in panel B.

Table S6: Data for experiment D. Irradiation time (t_{irr}) in seconds, absorbance at 378 nm (Abs) and molarity of NBD (C_{NBD}). Laser irradiation at 340 nm.

t_{irr}	Abs	C_{NBD}
0	0.868	7.95×10^{-3}
20	0.817	7.45×10^{-3}
40	0.768	6.95×10^{-3}
60	0.718	6.46×10^{-3}
80	0.667	5.95×10^{-3}
100	0.618	5.47×10^{-3}
120	0.567	4.95×10^{-3}
140	0.516	4.45×10^{-3}
160	0.466	3.95×10^{-3}
180	0.414	3.43×10^{-3}
200	0.363	2.92×10^{-3}
220	0.312	2.41×10^{-3}
240	0.261	1.90×10^{-3}
260	0.210	1.39×10^{-3}
280	0.159	8.87×10^{-4}
300	0.111	4.05×10^{-4}
320	0.076	5.74×10^{-5}
340	0.070	0
360	0.070	1.79×10^{-6}
380	0.071	1.37×10^{-5}
400	0.072	2.31×10^{-5}

$C_{total} = 7.95 \times 10^{-3}$ M, $\epsilon_{NBD,378nm} = 109.14$ $M^{-1}cm^{-1}$, $\epsilon_{QC,378nm} = 8.80$ $M^{-1}cm^{-1}$, $V = 0.00253$ L, $I = 0.0258$ W, $l = 1$ cm.

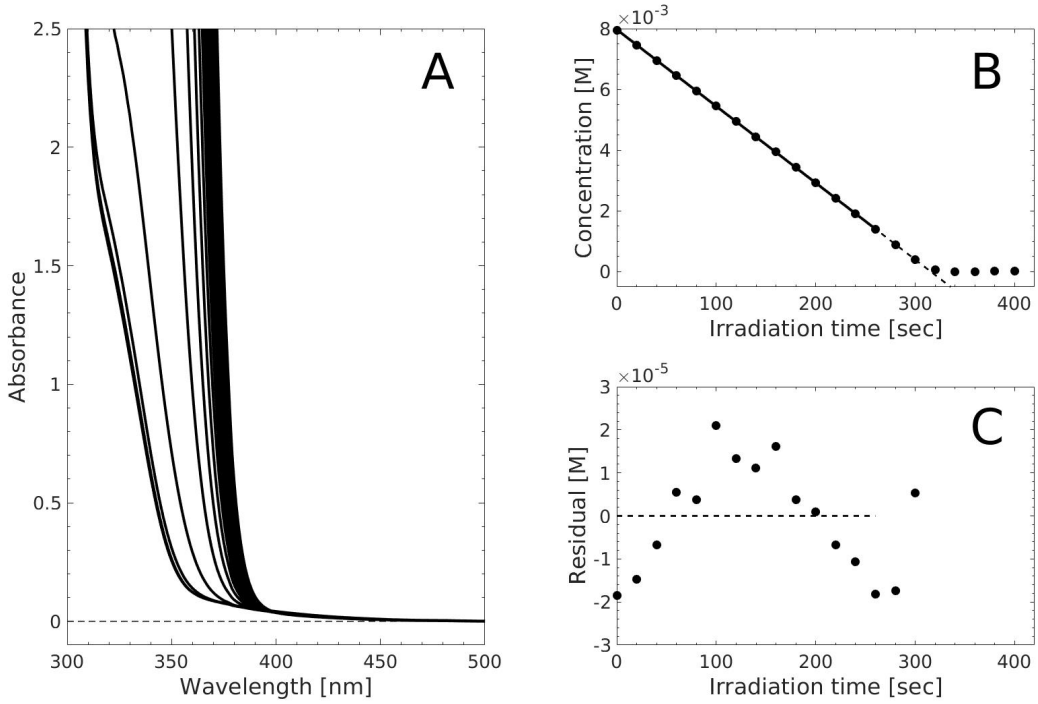

Figure S9: Experimental data plotted for experiment D from Table S6. **A**: Absorption spectra at various irradiation times. **B**: Concentration of NBD against irradiation time. **C**: Residual plot of the linear fit in panel B.

Table S7: Data for experiment E. Irradiation time (t_{irr}) in seconds, absorbance at 379 nm (Abs) and molarity of NBD (C_{NBD}). Laser irradiation at 340 nm.

t_{irr}	Abs	C_{NBD}
0	0.922	1.06×10^{-2}
50	0.814	9.24×10^{-3}
100	0.702	7.83×10^{-3}
150	0.570	6.18×10^{-3}
200	0.441	4.56×10^{-3}
250	0.307	2.87×10^{-3}
300	0.173	1.18×10^{-3}
350	0.080	1.15×10^{-5}
400	0.079	0
450	0.082	4.34×10^{-5}
500	0.081	2.75×10^{-5}
550	0.082	3.93×10^{-5}
600	0.083	5.55×10^{-5}

$C_{total} = 1.06 \times 10^{-2}$ M, $\epsilon_{NBD,379nm} = 87.00$ M^{-1}cm^{-1}, $\epsilon_{QC,379nm} = 7.42$ M^{-1}cm^{-1}, $V = 0.00207$ L, $I = 0.0287$ W, $l = 1$ cm.

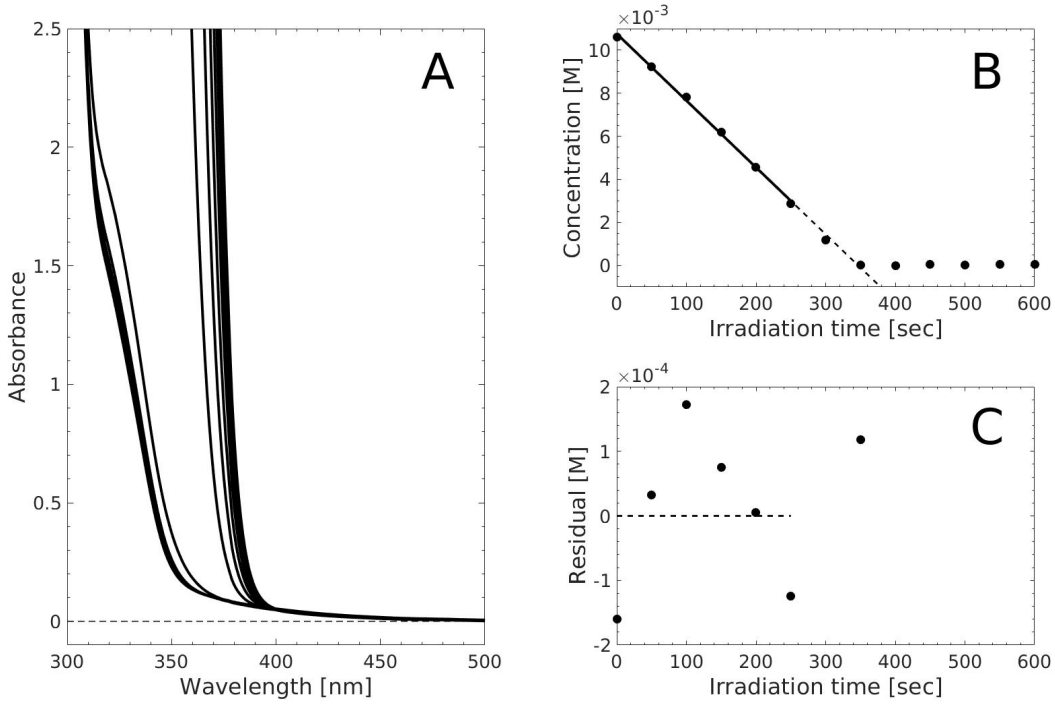

Figure S10: Experimental data plotted for experiment E from Table S7. **A**: Absorption spectra at various irradiation times. **B**: Concentration of NBD against irradiation time. **C**: Residual plot of the linear fit in panel B.

Table S8: Data for experiment F. Irradiation time (t_{irr}) in seconds, absorbance at 384 nm (Abs) and molarity of NBD (C_{NBD}). Laser irradiation at 340 nm.

t_{irr}	Abs	C_{NBD}
0	0.868	2.52×10^{-2}
50	0.836	2.40×10^{-2}
100	0.804	2.28×10^{-2}
150	0.771	2.16×10^{-2}
200	0.739	2.04×10^{-2}
250	0.705	1.91×10^{-2}
300	0.672	1.79×10^{-2}
350	0.640	1.67×10^{-2}
400	0.606	1.54×10^{-2}
450	0.574	1.42×10^{-2}
500	0.541	1.30×10^{-2}
550	0.508	1.18×10^{-2}
600	0.475	1.06×10^{-2}
650	0.443	9.34×10^{-3}
700	0.410	8.11×10^{-3}
750	0.377	6.90×10^{-3}
800	0.343	5.64×10^{-3}
850	0.311	4.42×10^{-3}
900	0.278	3.20×10^{-3}
950	0.247	2.06×10^{-3}
1000	0.219	1.01×10^{-3}
1050	0.197	1.83×10^{-4}
1100	0.192	0
1150	0.193	5.30×10^{-5}
1200	0.197	1.94×10^{-4}

$C_{total} = 2.52 \times 10^{-2}$ M, $\epsilon_{NBD,384nm} = 34.45$ $M^{-1}cm^{-1}$, $\epsilon_{QC,384nm} = 7.61$ $M^{-1}cm^{-1}$, $V = 0.00243$ L, $I = 0.0258$ W, $l = 1$ cm.

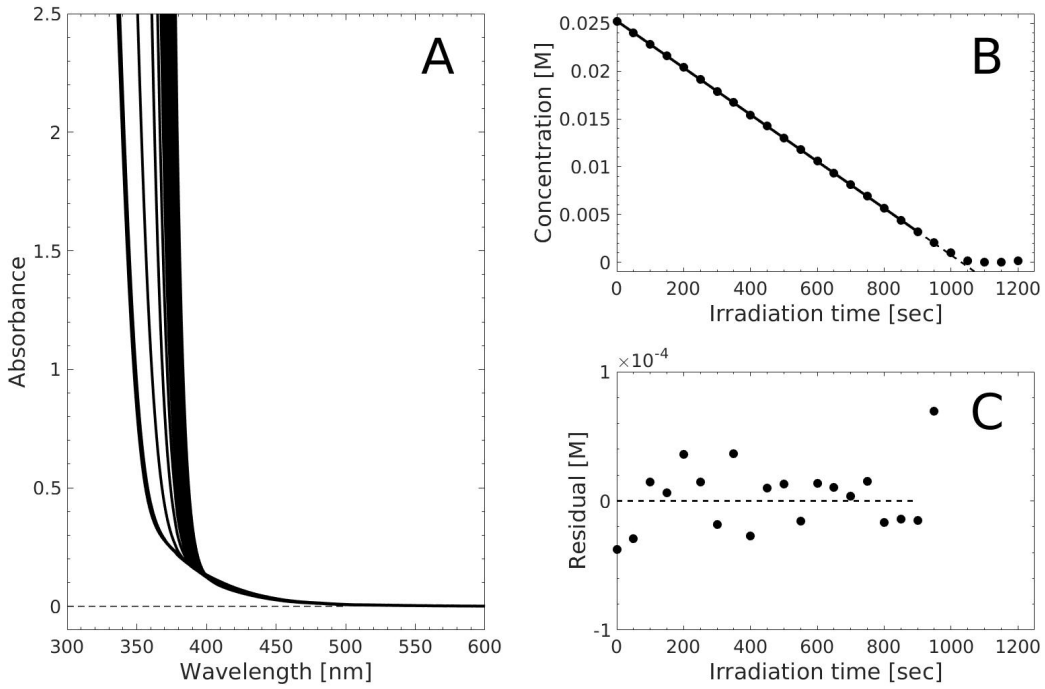

Figure S11: Experimental data plotted for experiment F from Table S8. **A**: Absorption spectra at various irradiation times. **B**: Concentration of NBD against irradiation time. **C**: Residual plot of the linear fit in panel B.

Table S9: Data for experiment G. Irradiation time (t_{irr}) in seconds, absorbance at 387 nm (Abs) and molarity of NBD (C_{NBD}). Laser Irradiation at 340 nm.

t_{irr}	Abs	C_{NBD}
0	0.986	5.00×10^{-2}
200	0.900	4.40×10^{-2}
400	0.820	3.84×10^{-2}
600	0.737	3.26×10^{-2}
800	0.648	2.64×10^{-2}
1000	0.567	2.08×10^{-2}
1200	0.473	1.43×10^{-2}
1400	0.390	8.51×10^{-3}
1600	0.304	2.55×10^{-3}
1800	0.268	0
2000	0.277	6.18×10^{-4}
2200	0.280	8.46×10^{-4}
2400	0.282	9.75×10^{-4}

$C_{total} = 5.00 \times 10^{-2}$ M, $\epsilon_{NBD,387nm} = 19.73$ M^{-1}cm^{-1}, $\epsilon_{QC,387nm} = 5.35$ M^{-1}cm^{-1}, $V = 0.00184$ L, $I = 0.0264$ W, $l = 1$ cm.

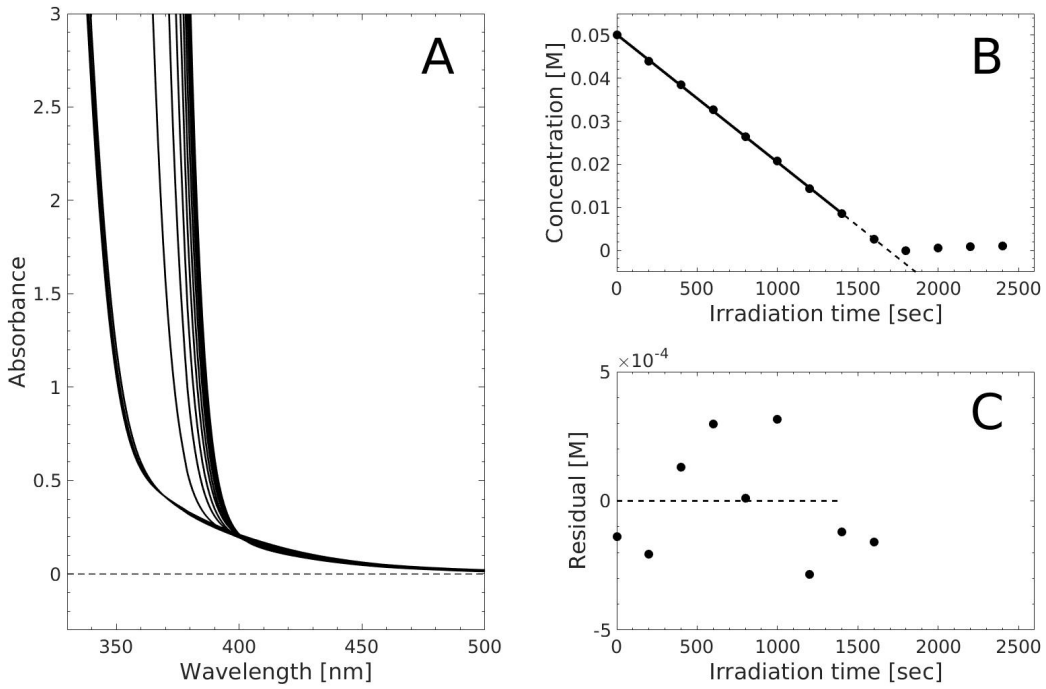

Figure S12: Experimental data plotted for experiment G from Table S9. **A**: Absorption spectra at various irradiation times. **B**: Concentration of NBD against irradiation time. **C**: Residual plot of the linear fit in panel B.

Table S10: Data for experiment H. Irradiation time (t_{irr}) in seconds, absorbance at 393 nm (Abs) and molarity of NBD (C_{NBD}). Laser Irradiation at 340 nm.

t_{irr}	Abs	C_{NBD}
0	0.962	1.02×10^{-1}
500	0.909	8.62×10^{-2}
1000	0.858	7.10×10^{-2}
1500	0.809	5.65×10^{-2}
2000	0.762	4.25×10^{-2}
2500	0.716	2.90×10^{-2}
3000	0.673	1.61×10^{-2}
3500	0.638	5.47×10^{-3}
4000	0.619	0
4500	0.632	3.74×10^{-3}
5000	0.643	6.95×10^{-3}
5500	0.653	9.95×10^{-3}
6000	0.662	1.27×10^{-2}

$C_{total} = 1.02 \times 10^{-1}$ M, $\epsilon_{NBD,393nm} = 9.43$ $M^{-1}cm^{-1}$, $\epsilon_{QC,393nm} = 6.07$ $M^{-1}cm^{-1}$, $V = 0.00208$ L, $I = 0.0265$ W, $l = 1$ cm.

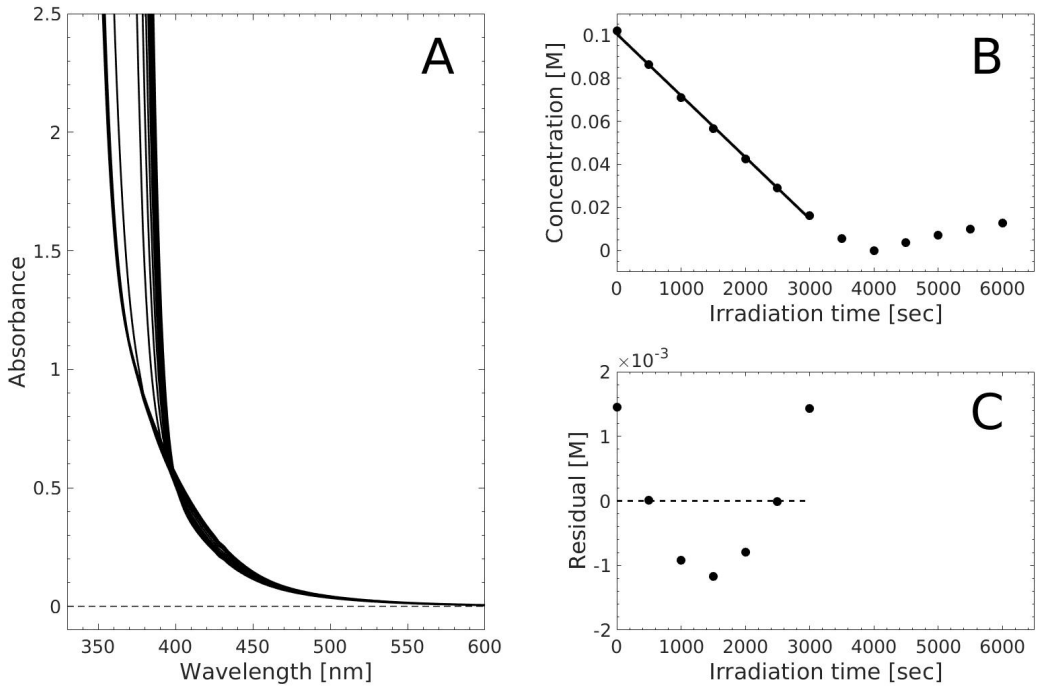

Figure S13: Experimental data plotted for experiment H from Table S10. **A**: Absorption spectra at various irradiation times. **B**: Concentration of NBD against irradiation time. **C**: Residual plot of the linear fit in panel B.

Table S11: Data for experiment I. Irradiation time (t_{irr}) in seconds, absorbance at 366 nm (Abs) and molarity of NBD (C_{NBD}). Laser irradiation at 310 nm.

t_{irr}	Abs	C_{NBD}
0	0.988	1.08×10^{-3}
5	0.921	1.01×10^{-3}
10	0.851	9.28×10^{-4}
15	0.782	8.52×10^{-4}
20	0.712	7.74×10^{-4}
25	0.643	6.97×10^{-4}
30	0.570	6.17×10^{-4}
35	0.501	5.40×10^{-4}
40	0.429	4.60×10^{-4}
45	0.357	3.80×10^{-4}
50	0.290	3.06×10^{-4}
55	0.224	2.32×10^{-4}
60	0.165	1.68×10^{-4}

$C_{total} = 1.08 \times 10^{-3}$ M, $\epsilon_{NBD,366nm} = 914.92$ $M^{-1}cm^{-1}$, $\epsilon_{QC,366nm} = 13.08$ $M^{-1}cm^{-1}$, $V = 0.00251$ L, $I = 0.0176$ W, $l = 1$ cm.

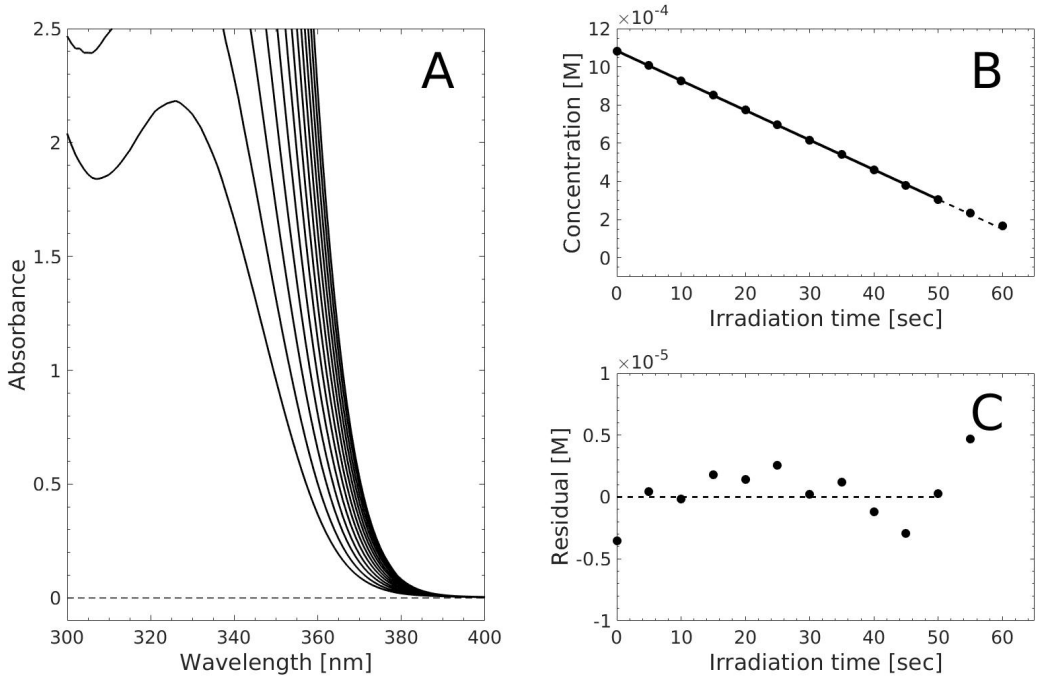

Figure S14: Experimental data plotted for experiment I from Table S11. **A**: Absorption spectra at various irradiation times. **B**: Concentration of NBD against irradiation time. **C**: Residual plot of the linear fit in panel B.

Table S12: Data for experiment J. Irradiation time (t_{irr}) in seconds, absorbance at 366 nm (Abs) and molarity of NBD (C_{NBD}). Laser irradiation at 320 nm.

t_{irr}	Abs	C_{NBD}
0	0.984	1.08×10^{-3}
5	0.882	9.66×10^{-4}
10	0.781	8.54×10^{-4}
15	0.681	7.42×10^{-4}
20	0.573	6.22×10^{-4}
25	0.472	5.09×10^{-4}
30	0.372	3.99×10^{-4}
35	0.267	2.82×10^{-4}
40	0.171	1.74×10^{-4}
45	0.088	8.23×10^{-5}
50	0.042	3.14×10^{-5}
55	0.024	1.11×10^{-5}
60	0.017	3.40×10^{-6}

$C_{total} = 1.08 \times 10^{-3}$ M, $\epsilon_{NBD,366nm} = 911.39$ $M^{-1}cm^{-1}$, $\epsilon_{QC,366nm} = 13.08$ $M^{-1}cm^{-1}$, $V = 0.00243$ L, $I = 0.0215$ W, $l = 1$ cm.

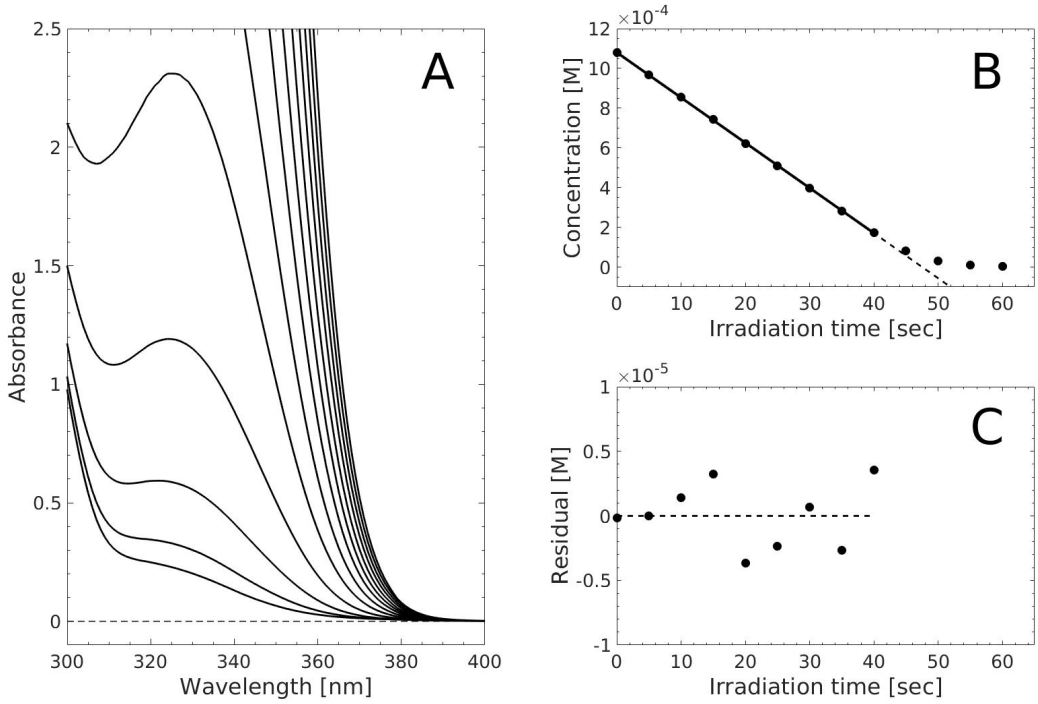

Figure S15: Experimental data plotted for experiment J from Table S12. **A**: Absorption spectra at various irradiation times. **B**: Concentration of NBD against irradiation time. **C**: Residual plot of the linear fit in panel B.

Table S13: Data for experiment K. Irradiation time (t_{irr}) in seconds, absorbance at 366 nm (Abs) and molarity of NBD (C_{NBD}). Laser irradiation at 330 nm.

t_{irr}	Abs	C_{NBD}
0	0.982	1.08×10^{-3}
5	0.900	9.89×10^{-4}
10	0.824	9.03×10^{-4}
15	0.742	8.12×10^{-4}
20	0.661	7.22×10^{-4}
25	0.581	6.33×10^{-4}
30	0.500	5.42×10^{-4}
35	0.419	4.52×10^{-4}
40	0.340	3.63×10^{-4}
45	0.260	2.74×10^{-4}
50	0.180	1.85×10^{-4}
55	0.110	1.06×10^{-4}
60	0.061	5.19×10^{-5}

$C_{total} = 1.08 \times 10^{-3}$ M, $\epsilon_{NBD,366nm} = 909.22$ $M^{-1}cm^{-1}$, $\epsilon_{QC,366nm} = 13.08$ $M^{-1}cm^{-1}$, $V = 0.00250$ L, $I = 0.0182$ W, $l = 1$ cm.

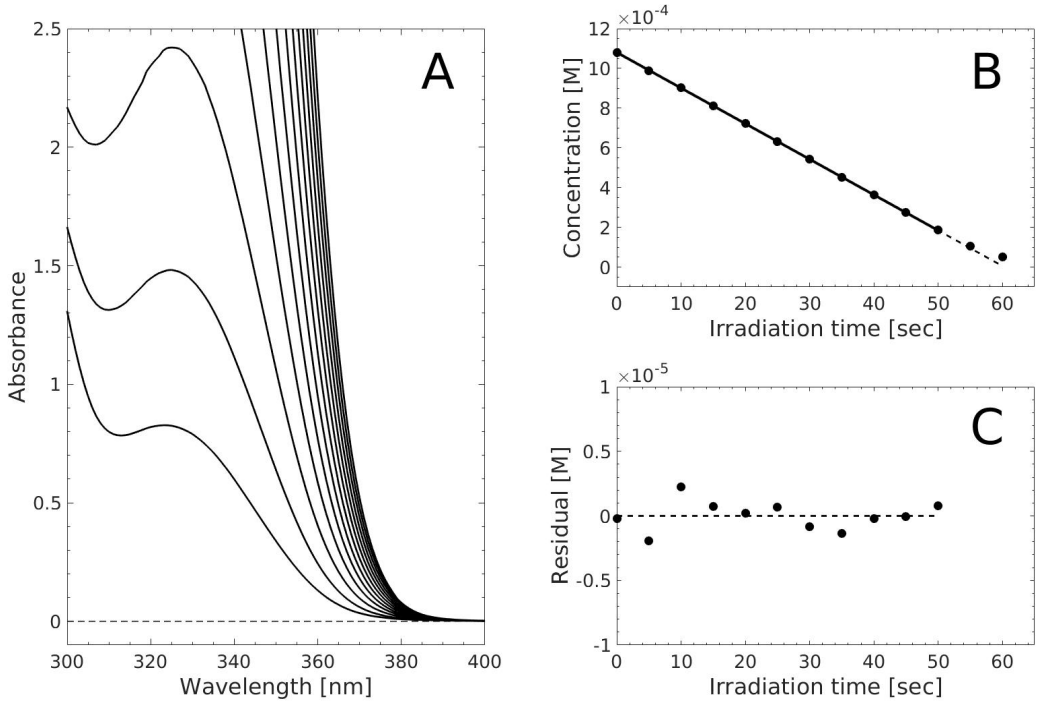

Figure S16: Experimental data plotted for experiment K from Table S13. **A**: Absorption spectra at various irradiation times. **B**: Concentration of NBD against irradiation time. **C**: Residual plot of the linear fit in panel B.

Table S14: Data for experiment L. Irradiation time (t_{irr}) in seconds, absorbance at 366 nm (Abs) and molarity of NBD (C_{NBD}). Laser irradiation at 350 nm.

t_{irr}	Abs	C_{NBD}
0	0.990	1.08×10^{-3}
5	0.909	9.91×10^{-4}
10	0.833	9.07×10^{-4}
15	0.754	8.19×10^{-4}
20	0.676	7.33×10^{-4}
25	0.597	6.45×10^{-4}
30	0.512	5.51×10^{-4}
35	0.433	4.63×10^{-4}
40	0.351	3.73×10^{-4}
45	0.278	2.92×10^{-4}
50	0.203	2.09×10^{-4}
55	0.141	1.41×10^{-4}
60	0.091	8.49×10^{-5}

$C_{total} = 1.08 \times 10^{-3}$ M, $\epsilon_{NBD,366nm} = 916.74$ $M^{-1}cm^{-1}$, $\epsilon_{QC,366nm} = 13.08$ $M^{-1}cm^{-1}$, $V = 0.00253$ L, $I = 0.0184$ W, $l = 1$ cm.

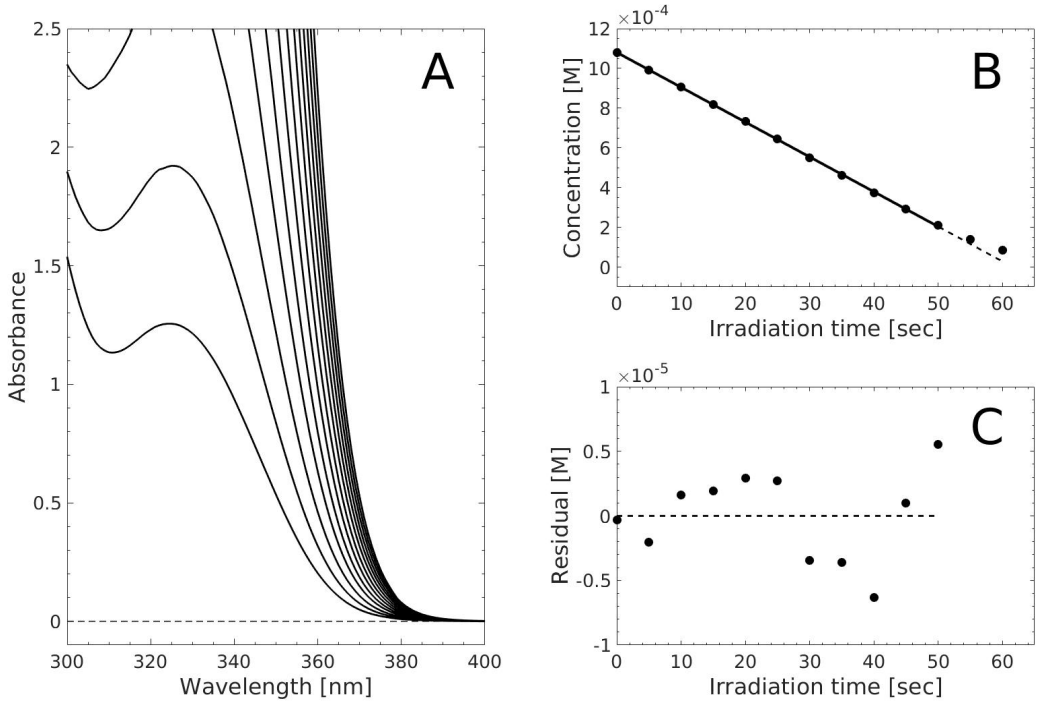

Figure S17: Experimental data plotted for experiment L from Table S14. **A**: Absorption spectra at various irradiation times. **B**: Concentration of NBD against irradiation time. **C**: Residual plot of the linear fit in panel B.

S6 ISOSun solar simulator

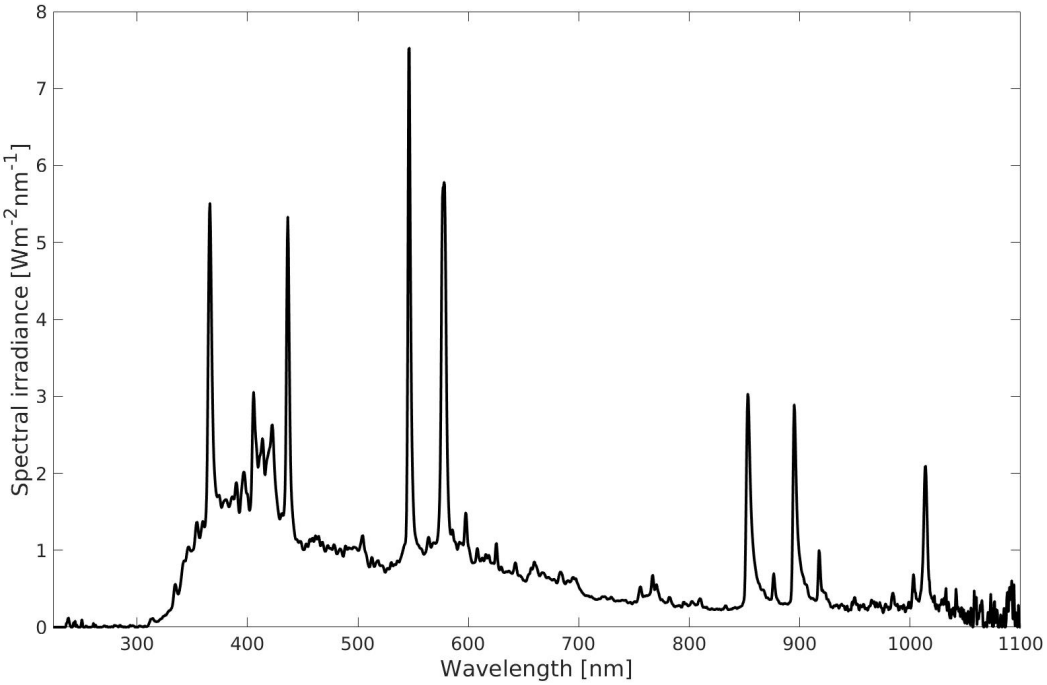

Figure S18: Spectral irradiance of the ISOSun, measured with the SolarRad at an irradiance of 640 W/m^2. ISOSun: Light adjustment: 0. Fan adjustment: 7, Photodiode: 0.231, Temperature: ∼317 K. The spectral intensities are measured without a cuvette between the lamp and the SolarRad, and are shown without corrections for the reflectance of the cuvette of 22%.

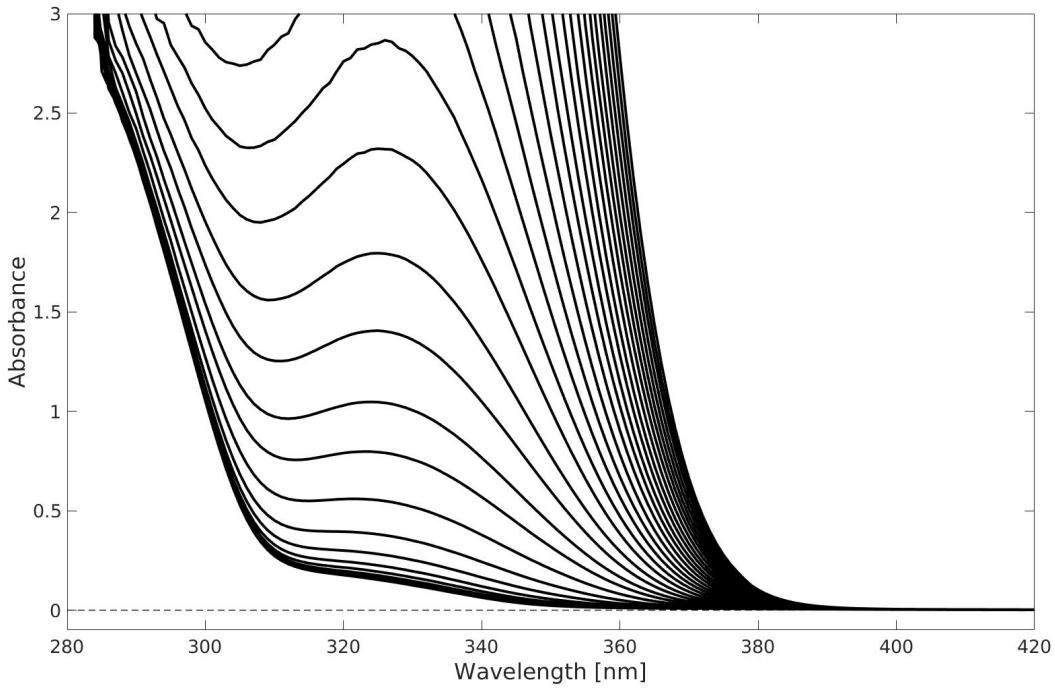

Figure S19: UV-Vis Absorption spectra of a 1.21×10^{-3} M solution in a 1-cm cuvette at irradiation times between 0 and 195 seconds, in steps of 5 seconds inside the ISOSun. A decrease in absorbance is observed at increasing irradiation time. The irradiance in the ISOSun was set to 640 W/m^2

Figure S20 shows the concentration of NBD against the irradiation time. Cubic splines are calculated and interpolated points are made every 0.01 seconds.

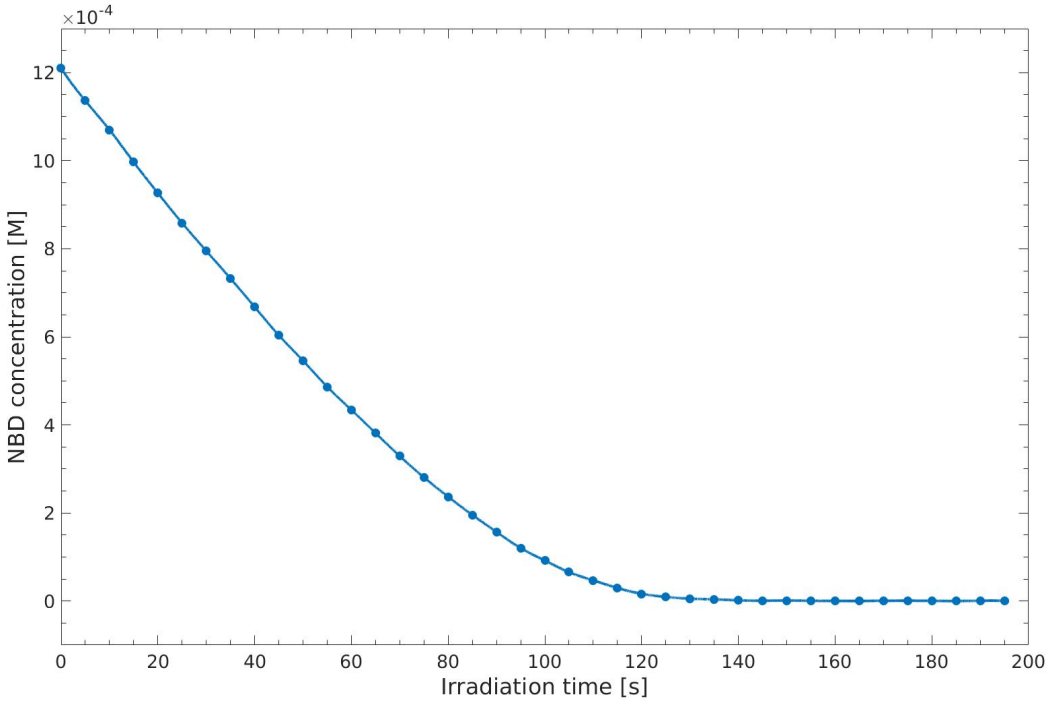

Figure S20: Concentration of NBD against irradiation time in the solar simulator. Sample of NBD at 1.21^{-3} M with concentrations determined every 5 seconds of irradiation in the ISOSun. The measurements were interpolated at every 0.01 seconds, using cubic splines (solid line). The irradiance in the ISOSun was set to 640 W/m^2.

Figure S21 shows the concentration gradient of the data in Figure S20. The concentration gradient ($C_{NBD}{}'$) is calculated as the average of the numerical left ($C_{NBD}{}'_{-}$) and right ($C_{NBD}{}'_{+}$) gradients, which are defined as:

$$\begin{aligned} C_{NBD-}(t_i)' &= \frac{C_{NBD}(t_{i-1}) - C_{NBD}(t_i)}{t_{i-1} - t_i} \\ C_{NBD+}(t_i)' &= \frac{C_{NBD}(t_i) - C_{NBD}(t_{i+1})}{t_i - t_{i+1}}, \end{aligned} \tag{S4}$$

where t_i, refer to the i'th data point for the irradiation time and $C_{NBD}(t_i)$ is the NBD concentration at an irradiation time of t_i.

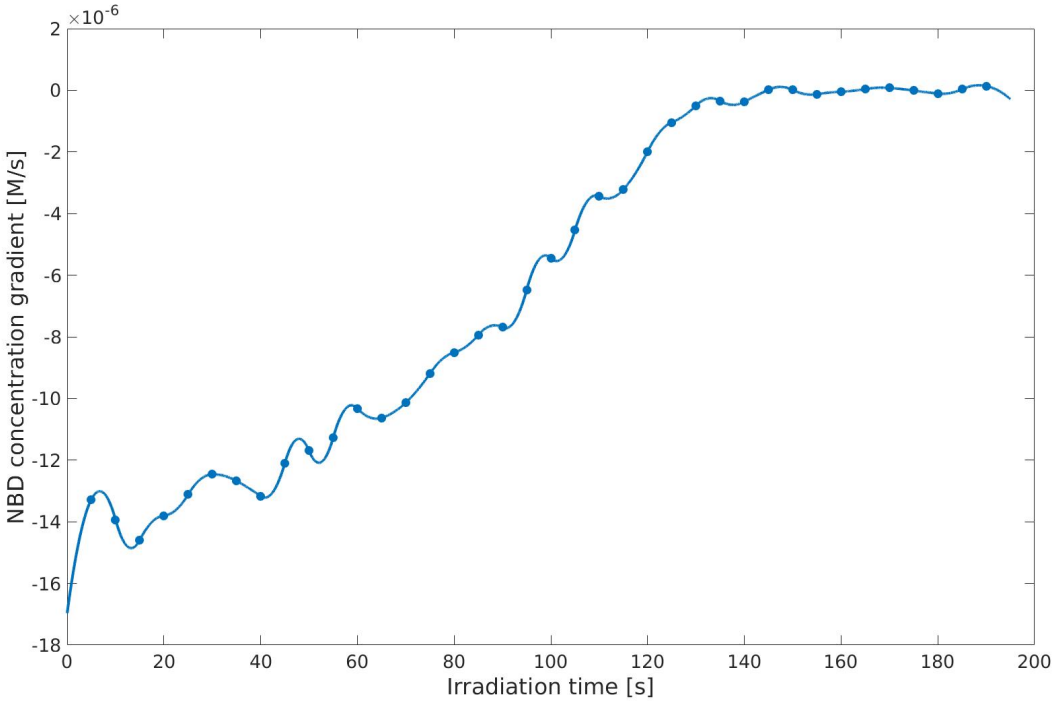

Figure S21: Concentration gradient of NBD against irradiation time. Concentration gradients were obtained from the average of the forwards and backwards concentration gradient (eq. (S4)), using the spline interpolation of the NBD concentration (Figure S20).

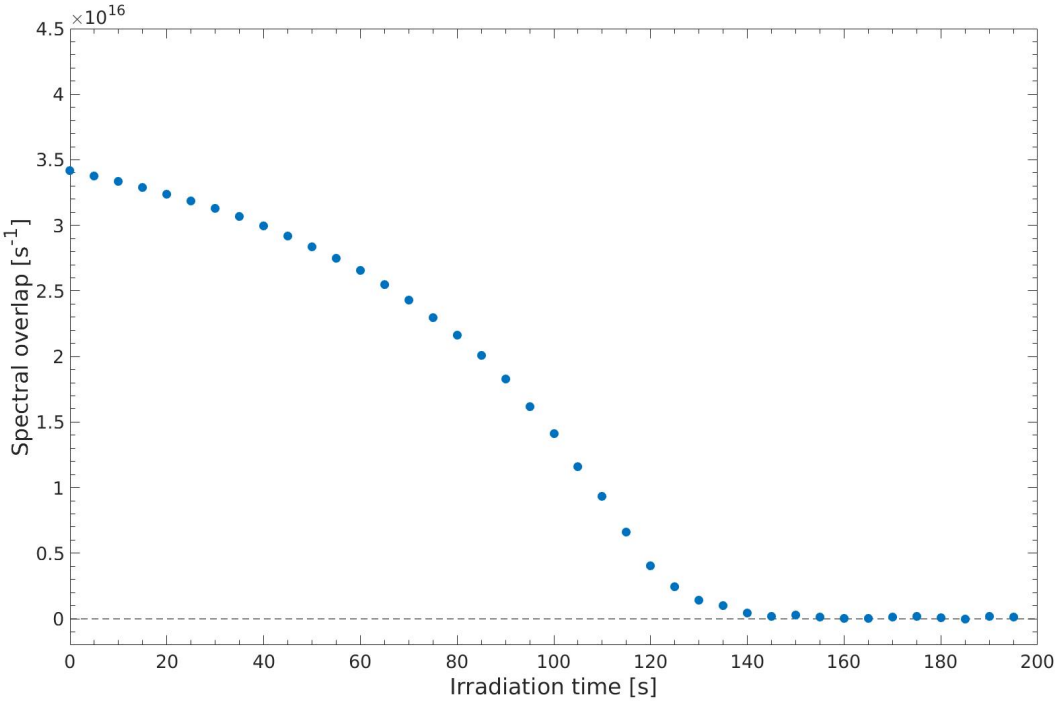

Figure S22: Spectral overlap of β_{NBD} with the ISOSun spectrum against irradiation time. The spectral overlap was integrated between 300 and 400 nm. Absorption spectra of NBD were obtained by multiplying time-dependent concentrations of NBD (section S6) with molar absorption coefficients of a low concentration NBD solution (table S16). Spectral photon flux have been multiplied by 0.72 to correct for the reflectance of the cuvette.

Table S15: Experimental data for the determination of $\phi_{NBD\rightarrow QC}$ in the ISOSun. In the table is given the irradiation time (t_{irr}) in seconds, the spectral overlap of β_{NBD} and spectral photon flux between 300-400 nm, at 640 W/m^2 ($\int \beta_{NBD} \times I(\lambda) d\lambda$) in s^{-1}, the concentration of NBD (C_{NBD}) in M, the concentration gradient of NBD ($C_{NBD}{}'$) in M/s and the absorbance at 368 nm (Abs). The sample volume was 3.89 mL. In the calculation of the spectral overlap, spectral photon fluxes have been multiplied by 0.72 to correct for a cuvette reflectance of 22%.

t_{irr}	$\int \beta_{NBD} \times I(\lambda) d\lambda^a$	C_{NBD}	${C_{NBD}}'^b$	Abs
0	$3.42 \cdot 10^{16}$	$1.21 \cdot 10^{-3}$	NaN	0.913
5	$3.38 \cdot 10^{16}$	$1.14 \cdot 10^{-3}$	$-1.33 \cdot 10^{-5}$	0.858
10	$3.34 \cdot 10^{16}$	$1.07 \cdot 10^{-3}$	$-1.39 \cdot 10^{-5}$	0.809
15	$3.29 \cdot 10^{16}$	$9.97 \cdot 10^{-4}$	$-1.46 \cdot 10^{-5}$	0.754
20	$3.24 \cdot 10^{16}$	$9.27 \cdot 10^{-4}$	$-1.38 \cdot 10^{-5}$	0.701

25	$3.18 \cdot 10^{16}$	$8.59 \cdot 10^{-4}$	$-1.31 \cdot 10^{-5}$	0.651
30	$3.13 \cdot 10^{16}$	$7.95 \cdot 10^{-4}$	$-1.25 \cdot 10^{-5}$	0.603
35	$3.07 \cdot 10^{16}$	$7.33 \cdot 10^{-4}$	$-1.27 \cdot 10^{-5}$	0.557
40	$3.00 \cdot 10^{16}$	$6.68 \cdot 10^{-4}$	$-1.32 \cdot 10^{-5}$	0.508
45	$2.92 \cdot 10^{16}$	$6.04 \cdot 10^{-4}$	$-1.21 \cdot 10^{-5}$	0.460
50	$2.84 \cdot 10^{16}$	$5.46 \cdot 10^{-4}$	$-1.17 \cdot 10^{-5}$	0.417
55	$2.75 \cdot 10^{16}$	$4.87 \cdot 10^{-4}$	$-1.13 \cdot 10^{-5}$	0.373
60	$2.65 \cdot 10^{16}$	$4.34 \cdot 10^{-4}$	$-1.03 \cdot 10^{-5}$	0.333
65	$2.55 \cdot 10^{16}$	$3.81 \cdot 10^{-4}$	$-1.06 \cdot 10^{-5}$	0.294
70	$2.43 \cdot 10^{16}$	$3.29 \cdot 10^{-4}$	$-1.01 \cdot 10^{-5}$	0.255
75	$2.30 \cdot 10^{16}$	$2.81 \cdot 10^{-4}$	$-9.19 \cdot 10^{-6}$	0.219
80	$2.16 \cdot 10^{16}$	$2.37 \cdot 10^{-4}$	$-8.51 \cdot 10^{-6}$	0.186
85	$2.01 \cdot 10^{16}$	$1.95 \cdot 10^{-4}$	$-7.94 \cdot 10^{-6}$	0.155
90	$1.83 \cdot 10^{16}$	$1.57 \cdot 10^{-4}$	$-7.69 \cdot 10^{-6}$	0.126
95	$1.62 \cdot 10^{16}$	$1.20 \cdot 10^{-4}$	$-6.47 \cdot 10^{-6}$	0.099
100	$1.41 \cdot 10^{16}$	$9.19 \cdot 10^{-5}$	$-5.44 \cdot 10^{-6}$	0.078
105	$1.16 \cdot 10^{16}$	$6.55 \cdot 10^{-5}$	$-4.54 \cdot 10^{-6}$	0.058
110	$9.31 \cdot 10^{15}$	$4.69 \cdot 10^{-5}$	$-3.44 \cdot 10^{-6}$	0.044
115	$6.64 \cdot 10^{15}$	$2.97 \cdot 10^{-5}$	$-3.22 \cdot 10^{-6}$	0.031
120	$4.05 \cdot 10^{15}$	$1.64 \cdot 10^{-5}$	$-1.99 \cdot 10^{-6}$	0.021
125	$2.44 \cdot 10^{15}$	$9.34 \cdot 10^{-6}$	$-1.04 \cdot 10^{-6}$	0.016
130	$1.43 \cdot 10^{15}$	$5.30 \cdot 10^{-6}$	$-4.98 \cdot 10^{-7}$	0.013
135	$1.02 \cdot 10^{15}$	$3.71 \cdot 10^{-6}$	$-3.46 \cdot 10^{-7}$	0.012
140	$4.29 \cdot 10^{14}$	$1.53 \cdot 10^{-6}$	$-3.75 \cdot 10^{-7}$	0.010
145	$1.89 \cdot 10^{14}$	$6.69 \cdot 10^{-7}$	$2.05 \cdot 10^{-8}$	0.009
150	$2.99 \cdot 10^{14}$	$1.06 \cdot 10^{-6}$	$9.81 \cdot 10^{-9}$	0.010
155	$1.57 \cdot 10^{14}$	$5.56 \cdot 10^{-7}$	$-1.26 \cdot 10^{-7}$	0.009

160	$4.51 \cdot 10^{13}$	$1.59 \cdot 10^{-7}$	$-4.65 \cdot 10^{-8}$	0.009
165	$2.89 \cdot 10^{13}$	$1.02 \cdot 10^{-7}$	$3.94 \cdot 10^{-8}$	0.009
170	$1.33 \cdot 10^{14}$	$4.72 \cdot 10^{-7}$	$7.62 \cdot 10^{-8}$	0.009
175	$1.86 \cdot 10^{14}$	$6.61 \cdot 10^{-7}$	$-8.30 \cdot 10^{-9}$	0.009
180	$1.04 \cdot 10^{14}$	$3.67 \cdot 10^{-7}$	$-1.06 \cdot 10^{-7}$	0.009
185	0	0	$3.39 \cdot 10^{-8}$	0.009
190	$1.82 \cdot 10^{14}$	$6.47 \cdot 10^{-7}$	$1.37 \cdot 10^{-7}$	0.009
195	$1.38 \cdot 10^{14}$	$4.89 \cdot 10^{-7}$	NaN	0.009

a: Spectral photon flux is obtained from the spectral irradiance multiplied with the surface area of a cuvette (3.7 cm^2).

b: Values of $C_{NBD}{}'$ were not determined (labeled as NaN) for the first (0 sec) and last recorded (195 sec) spectrum, as the forwards and backwards concentration gradient, respectively, cannot be calculated.

Table S16: The wavelength (λ) in nm and corresponding spectral photon flux (I) in $s^{-1}nm^{-1}$ of the 640 W/m^2 irradiance spectrum of the ISOSun and molar absorption coefficient (ϵ) in $M^{-1}cm^{-1}$ of a 6.3×10^{-5} NBD solution. Values of I in the table have been multiplied with the one-sided surface area of a cuvette (3.7 cm^2). Values of I in the table have been multiplied by 0.78 to correct for a cuvette reflectance of 22%.

λ	I	ϵ	λ	I	ϵ	λ	I	ϵ
300	$4.193 \cdot 10^{10}$	8216	334	$2.589 \cdot 10^{14}$	12496	368	$1.763 \cdot 10^{15}$	743.0
301	0^a	8451	335	$2.671 \cdot 10^{14}$	12225	369	$1.313 \cdot 10^{15}$	632.5
302	$6.985 \cdot 10^{12}$	8706	336	$2.307 \cdot 10^{14}$	11943	370	$1.097 \cdot 10^{15}$	537.3
303	$6.52 \cdot 10^{12}$	8960	337	$2.102 \cdot 10^{14}$	11629	371	$9.88 \cdot 10^{14}$	451.5
304	$3.256 \cdot 10^{12}$	9220	338	$2.207 \cdot 10^{14}$	11289	372	$9.258 \cdot 10^{14}$	377.0
305	$2.341 \cdot 10^{12}$	9492	339	$2.581 \cdot 10^{14}$	10928	373	$9.164 \cdot 10^{14}$	316.8
306	$1.415 \cdot 10^{12}$	9748	340	$3.152 \cdot 10^{14}$	10551	374	$9.346 \cdot 10^{14}$	264.6

307	$7.895 \cdot 10^{12}$	10013	341	$3.799 \cdot 10^{14}$	10152	375	$9.147 \cdot 10^{14}$	220.0
308	$1.214 \cdot 10^{12}$	10265	342	$4.205 \cdot 10^{14}$	9737	376	$8.598 \cdot 10^{14}$	180.3
309	$3.278 \cdot 10^{12}$	10509	343	$4.3 \cdot 10^{14}$	9315	377	$8.588 \cdot 10^{14}$	151.1
310	$9.372 \cdot 10^{12}$	10731	344	$4.315 \cdot 10^{14}$	8875	378	$8.875 \cdot 10^{14}$	124.1
311	$2.4 \cdot 10^{13}$	10939	345	$4.764 \cdot 10^{14}$	8429	379	$9.047 \cdot 10^{14}$	98.8
312	$4.273 \cdot 10^{13}$	11153	346	$5.188 \cdot 10^{14}$	7976	380	$9.148 \cdot 10^{14}$	82.7
313	$4.666 \cdot 10^{13}$	11364	347	$5.253 \cdot 10^{14}$	7523	381	$9.15 \cdot 10^{14}$	68.5
314	$5.269 \cdot 10^{13}$	11579	348	$5.066 \cdot 10^{14}$	7065	382	$8.93 \cdot 10^{14}$	54.7
315	$4.513 \cdot 10^{13}$	11808	349	$4.999 \cdot 10^{14}$	6609	383	$8.703 \cdot 10^{14}$	44.8
316	$3.603 \cdot 10^{13}$	12037	350	$5.067 \cdot 10^{14}$	6157	384	$8.837 \cdot 10^{14}$	39.2
317	$3.349 \cdot 10^{13}$	12269	351	$5.156 \cdot 10^{14}$	5710	385	$9.212 \cdot 10^{14}$	31.8
318	$3.33 \cdot 10^{13}$	12490	352	$5.569 \cdot 10^{14}$	5272	386	$9.494 \cdot 10^{14}$	25.1
319	$3.44 \cdot 10^{13}$	12696	353	$6.467 \cdot 10^{14}$	4850	387	$9.496 \cdot 10^{14}$	21.3
320	$4.055 \cdot 10^{13}$	12886	354	$7.031 \cdot 10^{14}$	4439	388	$9.369 \cdot 10^{14}$	18.4
321	$4.846 \cdot 10^{13}$	13048	355	$6.772 \cdot 10^{14}$	4038	389	$1.019 \cdot 10^{15}$	16.1
322	$5.085 \cdot 10^{13}$	13187	356	$6.139 \cdot 10^{14}$	3655	390	$1.066 \cdot 10^{15}$	12.6
323	$5.856 \cdot 10^{13}$	13302	357	$6.022 \cdot 10^{14}$	3295	391	$9.935 \cdot 10^{14}$	9.6
324	$6.632 \cdot 10^{13}$	13385	358	$6.491 \cdot 10^{14}$	2950	392	$8.725 \cdot 10^{14}$	8.5
325	$7.187 \cdot 10^{13}$	13437	359	$7.01 \cdot 10^{14}$	2630	393	$8.553 \cdot 10^{14}$	8.4
326	$7.081 \cdot 10^{13}$	13463	360	$7.155 \cdot 10^{14}$	2332	394	$9.64 \cdot 10^{14}$	5.8
327	$8.304 \cdot 10^{13}$	13454	361	$6.818 \cdot 10^{14}$	2060	395	$1.054 \cdot 10^{15}$	3.8
328	$9.369 \cdot 10^{13}$	13417	362	$7.2 \cdot 10^{14}$	1806	396	$1.14 \cdot 10^{15}$	3.4
329	$1.023 \cdot 10^{14}$	13337	363	$9.161 \cdot 10^{14}$	1579	397	$1.163 \cdot 10^{15}$	4.1
330	$1.052 \cdot 10^{14}$	13231	364	$1.561 \cdot 10^{15}$	1373	398	$1.094 \cdot 10^{15}$	3.3
331	$1.153 \cdot 10^{14}$	13097	365	$2.536 \cdot 10^{15}$	1187	399	$1.009 \cdot 10^{15}$	1.5
332	$1.343 \cdot 10^{14}$	12925	366	$2.929 \cdot 10^{15}$	1019	400	$1.005 \cdot 10^{15}$	0.9
333	$1.928 \cdot 10^{14}$	12726	367	$2.441 \cdot 10^{15}$	874			

a: Intensity below the noise threshold of the SolarRad. The intensity of the surrounding data points (5.376 $\times 10^{-10}$ $s^{-1}nm^{-1}$ and 8.955 $\times 10^{-12}$ $s^{-1}nm^{-1}$) are less than 1% of the peak intensity (3.755$\times 10^{15}$ $s^{-1}nm^{-1}$).

Figure S23: Photo of the InfinityPV ISOSun solar simulator.

Figure S23 shows the ISOSun solar simulator and Figures S24 to S26 illustrate the experimental setup used to determine the photoisomerization quantum yield with the solar simulator. Figure S24 shows the cuvette with the MOST solution in a small carton box. The cuvette was fastened to the box with a piece of tape. Figure S25 shows a photo of the

experimental setup with the solar simulator turned on. The top of the box is covered with foil and placed on a stirring plate in the solar simulator. The foil on top of the box was removed to irradiate the sample. The stirring plate was covered in foil to prevent it from overheating. For comparison, in Figure S26 the solar simulator is turned off, and we show the setup without the foil covering the stirring plate.

Figure S24: Cuvette with MOST fluid and stirring magnet placed in a small box. The cuvette is fastened to the box with a piece of tape on the screw-cap of the cuvette.

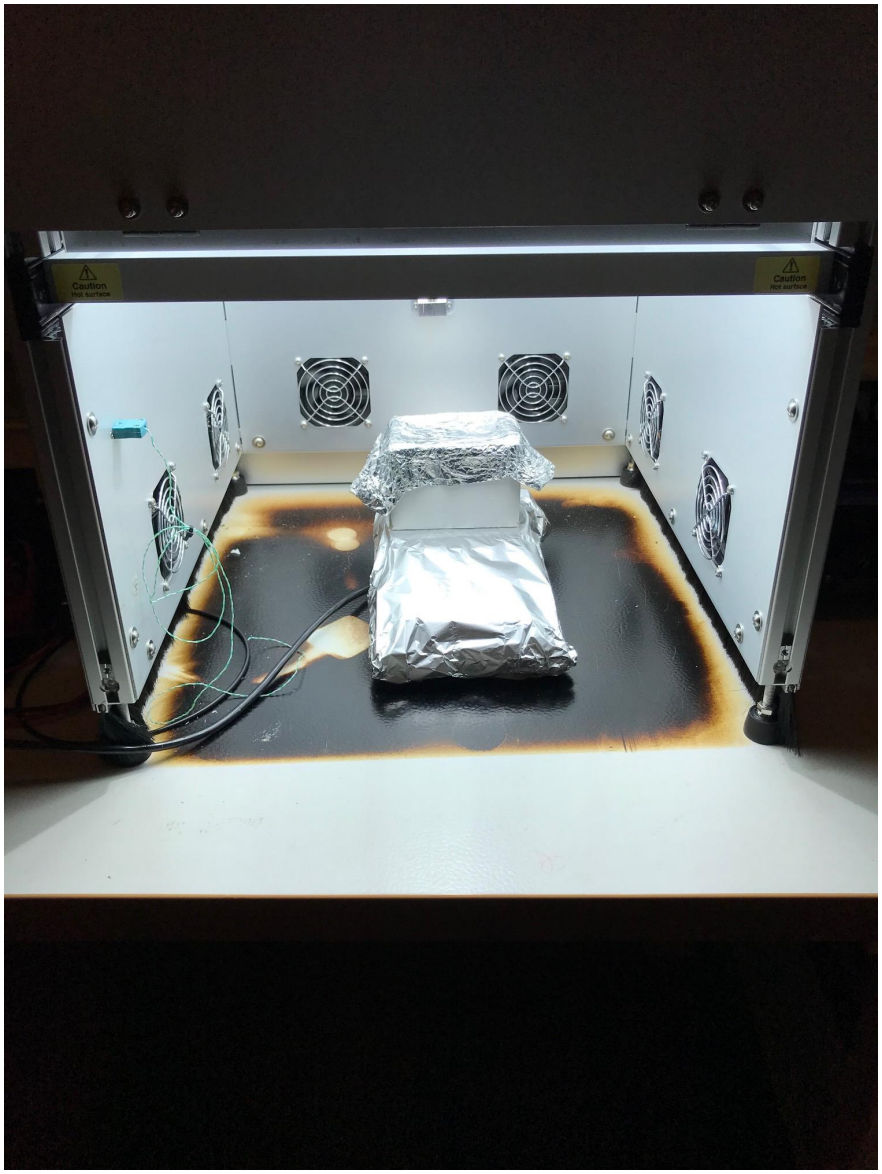

Figure S25: Setup for the determination of the photoisomerization quantum yield of the MOST fluid in the solar simulator. The lamp of the solar simulator is turned on, illuminating the area below. The stirring plate is covered with foil to prevent overheating, and the box with the cuvette is placed on top in the center of the illuminated area. Foil is placed on top of the box to block the light and is removed when the sample is irradiated.

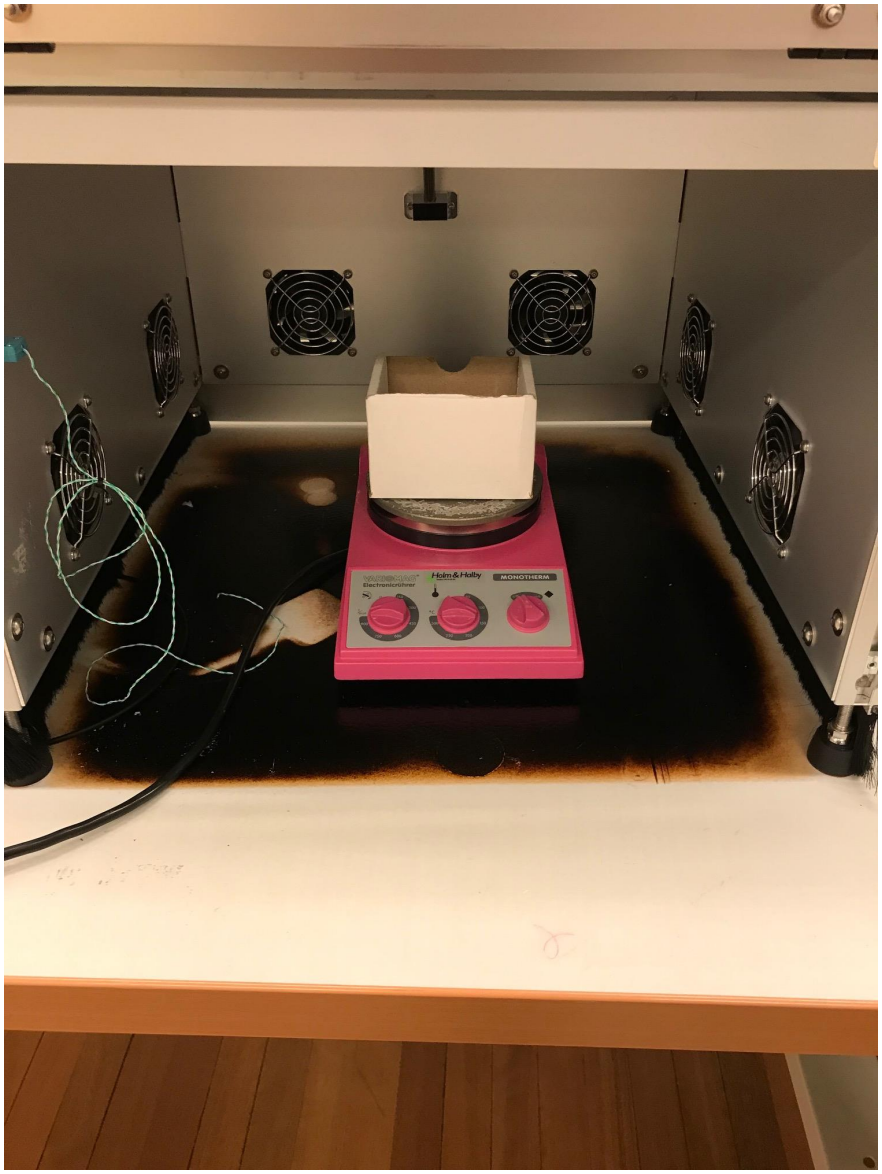

Figure S26: Stirring plate without foil covering the stirring plate and the box with the cuvette in the solar simulator. In the picture, the solar simulator was turned off. The green wire on the left side is the temperature probe, and the internal photodiode is placed on the back wall above the fans.

References

(1) Kuhn, H. J.; Braslavsky, S. E.; Schmidt, R. Chemical Actinometry. *Pure Appl. Chem.* **1989**, *61*, 187–210.

(2) Kuhn, H. J.; Braslavsky, S. E.; Schmidt, R. Chemical Actinometry (IUPAC technical report). *Pure Appl. Chem.* **2004**, *76*, 2105–2146.

(3) Stranius, K.; Börjesson, K. Determining the Photoisomerization Quantum Yield of Photoswitchable Molecules in Solution and in the Solid State. *Sci. Rep.* **2017**, *7*, 1–9.